2022 44th Annual International Conference of
the IEEE Engineering in Medicine & Biology Society (EMBC)
Scottish Event Campus, Glasgow, UK, July 11-15, 2022

2022 44th Annual International Conference of the IEEE Engineering in Medicine & Biology Society (EMBC) | 978-1-7281-2782-8/22/$31.00 ©2022 IEEE | DOI: 10.1109/EMBC48229.2022.9871415

Excitation coil for sentinel lymph node harvesting: design, digital twin and prototype*

L. Molenaar, M.M. Horstman – van de Loosdrecht, H.J.G. Krooshoop,
R.J.H. Wesselink, B. ten Haken, I.A.M.J. Broeders, and L. Alic

***Abstract*—A recently developed prototype (Laparoscopic Differential Magnetometer, in short LapDiffMag) identifies magnetic tracer accumulated inside sentinel lymph nodes (SLNs) during clinical laparoscopic procedures. The LapDiffMag relies on excitation of superparamagnetic iron oxide nanoparticles (SPIONs) and subsequent laparoscopic detection based on a nonlinear detection principle. The prototype uses an excitation coil to generate a magnetic field needed to activate SPIONs. This study reports on the process of developing a new excitation coil by describing the design choices based upon clinical requirements, by modeling delivered magnetic field using digital twin, and by comparing the magnetic fields of modeled and manufactured prototype. Digital twin technology was used to produce relevant and reliable data to demonstrate the safety and effectiveness of the excitation coil. The magnetic field originating from manufactured prototype was validated at two different heights above the excitation coil and have shown a good concordance to the data generated by its digital twin.**

***Clinical Relevance*— Current standard-of-care for a variety of tumor types consists of minimally invasive radical resection of primary tumor and regional lymph nodes (LNs). The newly introduced excitation coil will (after full validation) enable minimally invasive harvesting of sentinel LNs by means of magnetic tracer detection.**

I. Introduction

For most primary tumor types with a high risk of metastases, current standard-of-care consists of minimal invasive radical resection of the primary tumor and regional lymph nodes (LNs). Within these regional LNs, the first tumor draining LNs (referred to as sentinel lymph nodes, SLNs) have an increased probability to contain metastases. As metastases lead to a low patient survival [1], the presence of metastases is therefore an important prognostic factor and is used for treatment planning. However, given retrospective absence of metastases in LNs after pathology, complete removal of regional LNs leads to unnecessary costs, added patient burden and possible complications without clear patient benefit. The sentinel lymph node biopsy (SLNB) uses a tracer (for example radioactive, fluorescent, magnetic, or a hybrid) to identify SLNs after tracer injection around the primary tumor [2]. These tracers are usually non-specific, i.e. they follow the natural lymphatic pathways, without binding on specific (tumor) cells. SLN identification is done by using a tracer-specific intraoperative detector, and subsequent resection for pathological confirmation. By using the SLNB on a patient group with a known overall low number of metastases, a large group of patients can be treated by primary tumor removal and resection of a low number of SLNs instead of all regional LNs. This decreases the complication chance and patient discomfort [3]. The effectiveness of SLNB is currently being investigated for several types of cancers suitable for a laparoscopic procedure [4], e.g. esophagus cancer, gastric cancer, colon cancer, prostate cancer, bladder cancer, and endometrial cancer [5-10]. A recently developed prototype (Laparoscopic Differential Magnetometer, in short LapDiffMag) is suitable to identify the magnetic tracer inside SLNs during clinical laparoscopic procedures [11].

The LapDiffMag relies on excitation of superparamagnetic iron oxide nanoparticles (SPIONs) by a strong magnetic field [12] and laparoscopic detection based on a nonlinear detection principle [13]. The excitation coil of the first benchtop prototype has a circular configuration, an outer diameter of 270 mm, a height of 10 mm, and produces a sufficient magnetic field enabling detection up to 200 mm above its surface [14]. Validating this prototype against clinical requirements (in terms of iron content sensitivity, depth and spatial sensitivity, and angular sensitivity) revealed a necessity for a larger excitation coil that would increase the size of a sufficiently strong magnetic field to at least 300 x 300 x 300 mm. This larger magnetic field will allow clinical use in abdominal and thoracic applications.

This study reports on the process of developing a new excitation coil by describing the design choices, a computer model of the magnetic field and compare this with magnetic field tests, and prototype manufacturing. The choice was made to create a new prototype with a magnetic field as large as possible within determined physical boundaries (length and width), to prevent technical limitations in a clinical application. The design of the excitation coil involved the creation of a digital twin. Digital twin technology (DTT) was used to produce relevant and reliable data to demonstrate the safety and effectiveness of the excitation coil. The use of DTT accelerated development and provided a fast and inexpensive option to anticipate and prevent errors. DTT is also accepted as evidence in the regulatory process of medical devices. Finally, the simulated results were compared with the experimental data [15].

*This research has been sponsored by the Netherlands Organization for scientific Research (NWO), under the research program Magnetic Sensing for Laparoscopy (MagLap), with project number 14322.

L. Molenaar, M.M. Horstman – van de Loosdrecht, H.J.G. Krooshoop, B. ten Haken, and L. Alic are with the Magnetic Detection & Imaging group, Technical Medical Centre, University of Twente, Enschede, The Netherlands (corresponding author: L. Alic, l.alic@utwente.nl).

R.J.H. Wesselink is with DEMCON, Enschede, The Netherlands.

I.A.M.J. Broeders is with the Department of Surgery, Meander Medical Center, Amersfoort, The Netherlands and Robotics and Mechatronics group, University of Twente, Enschede, The Netherlands.

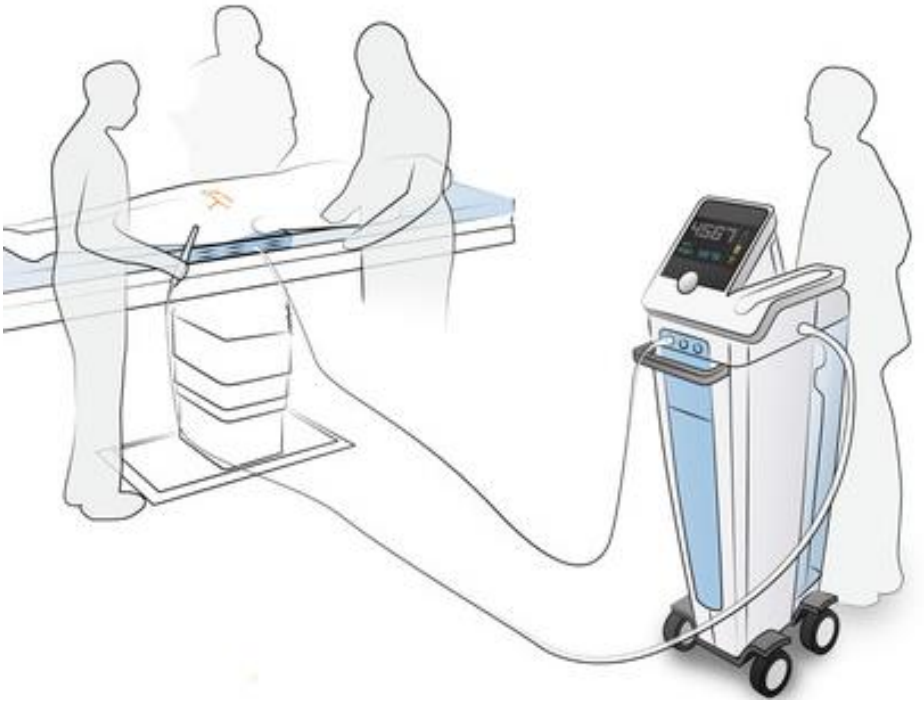

Figure 1. A graphical representation of an excitation coil, a detection probe and a control unit.

II. METHODS

A. Design

The complete LapDiffMag system consists of three main parts [11, 14]: a set of excitation coils, a detection probe, and a control unit (Fig. 1). There are two coils needed to create the magnetic excitation field: a coil to generate a low-frequent (LF) field and a coil to generate a high-frequent (HF) field. The excitation coil is designed to be placed underneath a patient. Passive and active thermal cooling will be necessary to produce a coil conform safety norms (e.g. prevent burn wounds) and prevent damage of the coil itself. Moreover, the temperature needs to be continuously monitored to guarantee safety. In a clinical scenario the top of the coil would be covered by a matrass for patient comfort, complicating thermal dissipation, and underlining the need for effective cooling. Therefore, the excitation coil design includes an internal temperature sensor and a ventilator. The detection probe consist of two coils to detect the magnetic signal and two coils to compensate for the magnetic field generated by the excitation coil. The probe is designed to be operated by a laparoscopic surgeon and already tested with a clinical setting in mind [11]. The control unit consists of multiple parts: two power supplies, a transformer, a series resonant circuit, safety equipment, and a data acquisition system. The series resonant circuit is used to get the high working voltage on the HF-coil. The transformer consists of three coils: one coil to create the HF-field and two coils to create the LF-field. This transformer must have the same mutual inductance between HF- and LF-sections as the excitation coil in order to work properly, but can vary in physical properties. The transformer also uncouple the HF- and LF-coil, i.e. it prevents induction of a voltage in the LF-coil by the HF-coil. Both excitation coils (LF and HF) are designed to operate with an AE TECHRON-7228 power supply.

The following design parameters were addressed to guarantee clinical requirements (e.g. magnetic field size and maximum operating temperature), electromagnetic safety, and technical functioning:

- Coil design necessary to create a magnetic field of 300 x 300 x 300 mm enabling SPION detection of ≥50 µg [11].
- Coil dimensions fitting mainstream operation room (OR) tables (average width of 520 mm), with a minimal thickness.
- The isolation of excitation coil (needed for electrical protection), suited to be sterilized for clinical use and enabling passive and active thermal cooling.

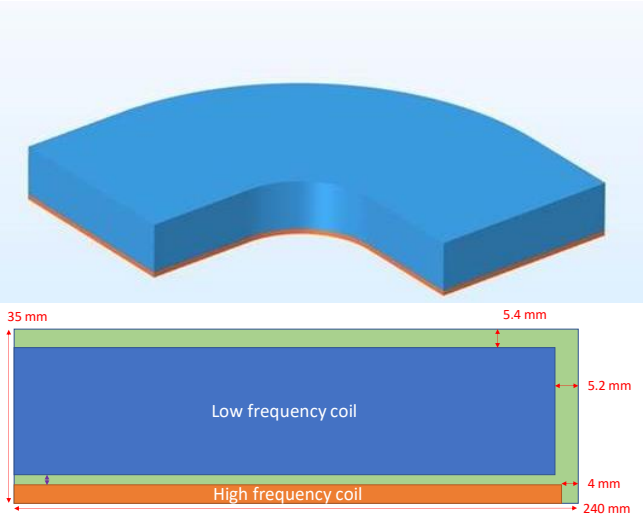

Figure 2. Schematic of one quarter of the proposed excitation coil.

B. Digital Twin

Based upon Maxwell-equations, a finite element method digital twin model was implemented (COMSOL Multiphysics® v.5.5, COMSOL AB, Stockholm, Sweden). The coils are modelled using a homogenized multitum approach, avoiding the need for modelling each individual turn. The total number of ampere-turns in the coil cross section is thus imposed in the form of a homogeneous current density that amounts to the same total current. Fig. 2 shows a schematic of the proposed model (including its physical dimensions) of one quarter of the excitation coil. This digital twin was used to finalize the design of the excitation coil.

C. Prototype

Designing and manufacturing this new excitation coil is a specialized process. The copper coils of the excitation coil and transformer were wet-wound by hand using an epoxy resin due to their size and uniqueness. The total number of windings used for the excitation coil is 196 for the LF-coil and 40 for the HF-coil, with a wire diameter of 4.1 and 2.9 mm respectively. All coils are made with Litz wire to reduce the skin effect, eddy currents, and proximity effect losses [16]. Specifically, current in a solid copper cable is concentrated at the periphery. Furthermore, for high frequencies the current migrates to the surface. The multiple strand construction of Litz allows current to divide uniformly between strands, reducing the skin effect. Eddy currents are produced by an alternating magnetic field, which also alters the overall distribution of current in the windings, and consequently might produce heat. The used mold for manual wet-wounding of the coils was also custom made to fit the necessary size and thickness. The cover for the excitation coil was 3D-printed in PA (nylon) and coated for protection and hygienic purposes.

D. Validation experiments

This study shows the first magnetic LF measurements as a preliminary test. To validate the LF magnetic field of the manufactured coil prototype, the acquired field data was compared to the modelled magnetic field and was validated in the points illustrated in Fig. 3.

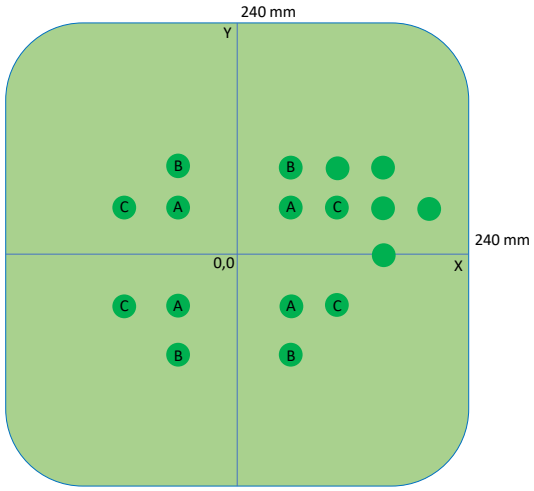

Figure 3. Points measured on 5 mm height above coil surface (Z1). All 8 points in the right upper quadrant were also measured at 106 mm height above coil surface (Z2). Point A, B, and C were measured in every quadrant.

Both numerical model and manufactured prototype (X = length, Y = width, Z = height) were powered by a current of 1.65 A. The magnetic field at Z1 = 5 mm, and Z2 = 106 mm were acquired. A number of acquisitions were repeated in all quadrants for a quadrant comparison. The magnetic field was measured with a Tesla meter (FM302 with AS-NTM-2 transverse probe, ProjectEL). This Tesla meter only measures the magnetic field perpendicular on the probe, i.e. only the perpendicular magnetic field component (B_Z) will be measured. The center of the coil (X, Y, Z = 0, 0, 0) is chosen at the top of the casing. For validation purposes, COMSOL-data at the selected points was also exported.

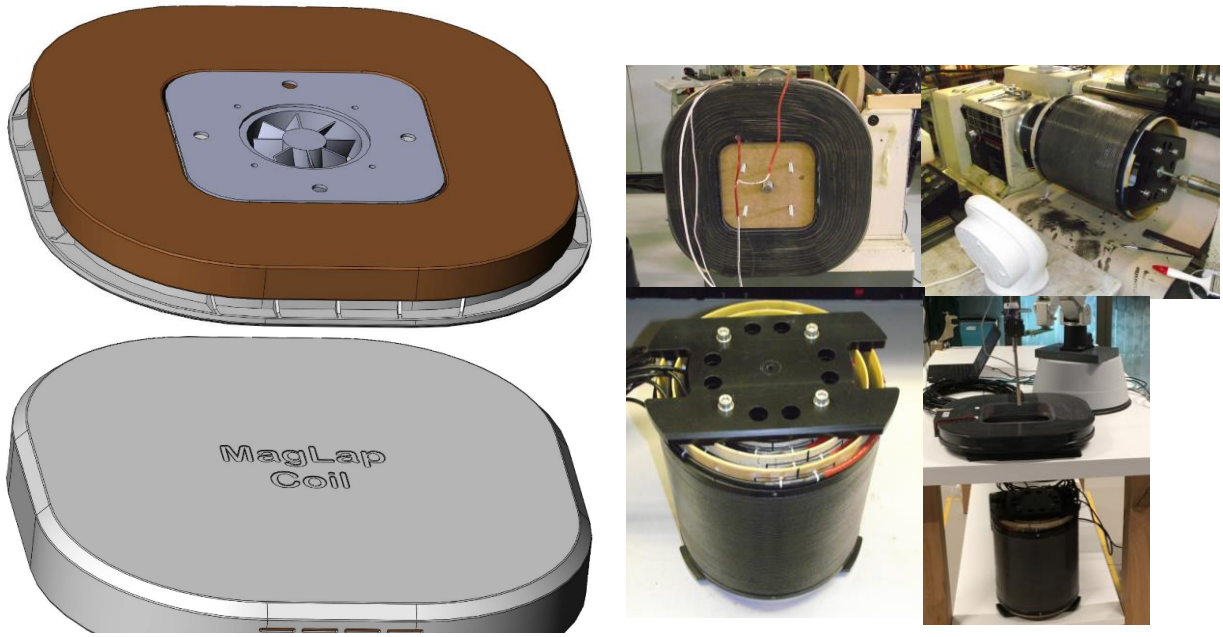

Figure 4: On the left the prototype excitation coil with its cover. On the right several images of the prototype process: wet-wounding of the coils, assemblage of coils and a measurement setup.

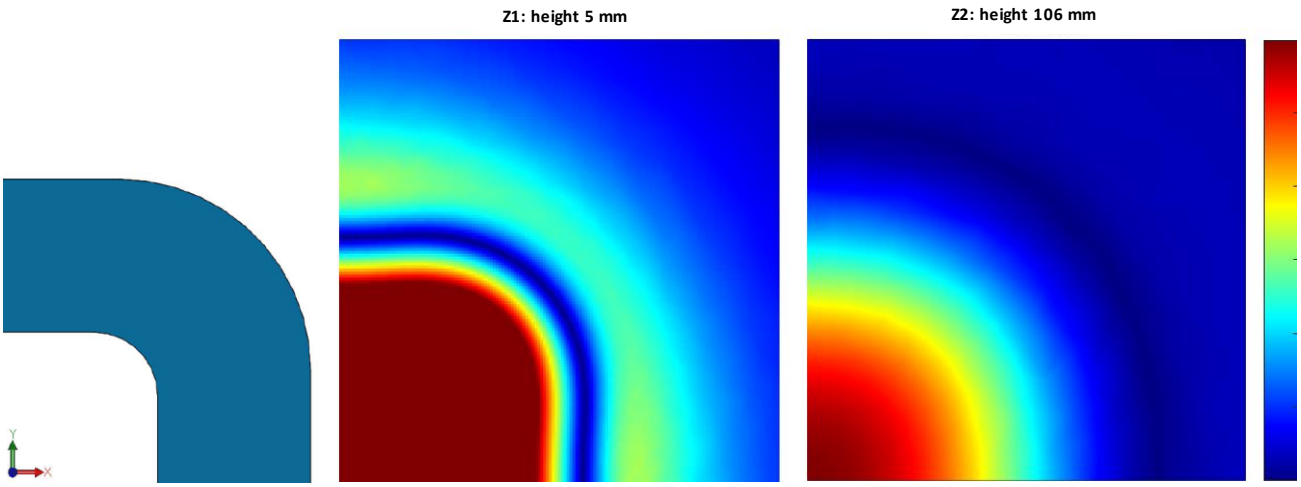

Figure 5: Varying simulated magnetic fields based on the COMSOL model: on the left quarter of the execution coil as reference, in the middle and on the right the magnetic field at 5 and 106 mm.

III. Results

A. Design & prototype

Both the excitation coil and transformer are placed inside a cover for electrical safety. To fit the new excitation coil on a mainstream OR table, the length and width of the coil cover was designed at 520 x 520 mm enabling a magnetic field coverage of (at least) 300 x 300 x 300 mm. The total height (including cover and legs) is 115 mm. The excitation coil fits comfortably inside the 3D-printed plastic cover case (length/width/height = 480/480/35 mm). The diameter and height of the transformer cover is 330 mm and 640 mm respectively, and the transformer itself has a diameter of 285 mm with a height of 391 mm.

The cover for both the excitation coil and transformer were designed to enable passive heat dissipation (air slits were added). A fan was added as active cooling component. In addition, multiple temperature sensors (PT100) were added for monitoring. The system is designed to switch the power supplies to standby when the temperature exceeds 40°C, and to completely shut-down the system when temperature exceeds 45°C. Fig. 4 show parts of the design and production process.

B. Digital Twin

Prior to manufacturing the prototype, the numerically simulated results were checked for safety reasons. The observed magnetic field within the physical boundaries of the excitation coil at the cover height ranged 0-1.6 mT, while at the height of 106 mm above the cover ranged 0-0.4 mT. The maximum remaining magnetic field outside the 300 mm was 5 µT.

C. Validation experiments

As shown in Fig. 3, 17 points were measured at 5 mm and 8 points were measured at 106 mm above the casing. The Bland-Altman plot in Fig. 6 illustrates a good consistency between the COMSOL-modeled field and a measured magnetic field. The mean and standard deviations were calculated for the three points measured at all four quadrants at Z = 5 mm (A = 1.222 mT ± 0.036 mT, B = 0.152 mT ±

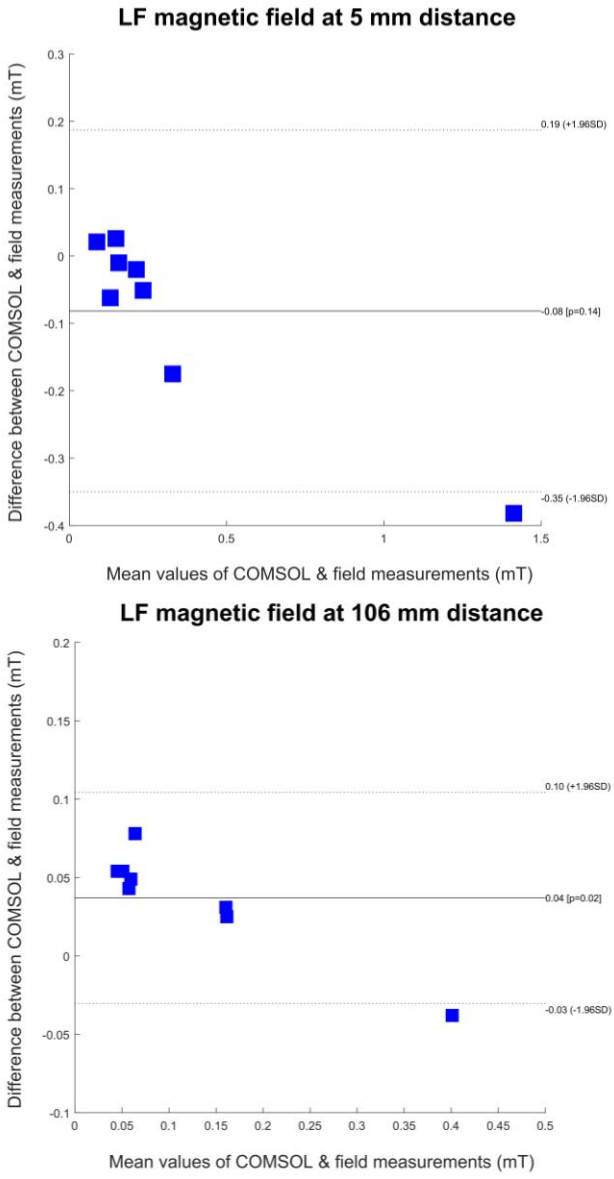

Figure 6: Bland-Altman plot of all measurements at 5 mm (upper figure) and at 106 mm (lower figure)

0.033 mT, and C = 0.099 mT ± 0.030 mT). The maximum measured magnetic field at 5 mm distance was 1.22 mT and was decreasing to 0.38 mT at the height of 106 mm.

IV. Discussion

The excitation coil for SLNB in a laparoscopic procedure that fits clinical requirements demonstrated a good concordance between modelled and measured magnetic fields (Fig. 6). At both heights, one outlier is present. An increased number of measurements are necessary to differentiate between possible measurement errors and true deviations. Furthermore, it appears that increasing distance from the centre of the coil while keeping the Z-distance constant decreases the magnetic field (both in DTT and experimental data). This could be explained by the direction of the magnetic field lines (which bend around the surface of the coil) and the fact we only measure the magnetic field perpendicular to the excitation coil. When only increasing the Z-distance, the magnetic field lines will turn slightly more perpendicular, increasing the magnetic field measured. Quadrant comparison of the excitation coil resulted in low standard deviations (0.036, 0.033, and 0.030 mT) illustrating a good comparability between all four coil quadrants.

The current prototype was designed to create a large magnetic field, presumably larger than clinical necessary. Consequently, the total thickness of the excitation coil (including cover) is 115 mm. Since the length and width fits on all mainstream OR tables and encompass most patients, no length/width changes are desired. Incorporation of the coil on an operating table is possible, although a thinner and lighter coil is more preferable. Future work will focus on a minimally viable product supporting a excitation field enabling measurement of clinically relevant amounts of magnetic tracer by e.g. minimising coil thickness.

In conclusion, this study shows promising first results regarding excitation coil for sentinel lymph node harvesting. A future extensive comparison between the excitation coil and its digital twin is necessary to fully assess the prototype. These experiments will cover clinical relevant currents to create sufficient magnetic field mimicking the clinical circumstances. That also includes a high number of individual measurements in every quadrant at several heights up to 40 cm, for both the LF- and HF-field. Furthermore, in addition to acquiring the magnetic field perpendicular to the excitation coil, the experiments will also include more realistic 3D acquisitions relevant for a laparoscopic surgery that utilize varying angles (not only perpendicular to the execution coil).

Acknowledgment

The authors would like to thank Panton, Thijs van Asselt, and Sven Tesselaar for their contribution to this research.

References

[1] Sloothaak, D., et al., *The prognostic value of micrometastases and isolated tumour cells in histologically negative lymph nodes of patients with colorectal cancer: a systematic review and meta-analysis.* European Journal of Surgical Oncology (EJSO), 2014. **40**(3): p. 263-269.

[2] Kim, T., A.E. Giuliano, and G.H. Lyman, *Lymphatic mapping and sentinel lymph node biopsy in early-stage breast carcinoma: a metaanalysis.* Cancer, 2006. **106**(1): p. 4-16.

[3] Amersi, F. and N.M. Hansen, *The benefits and limitations of sentinel lymph node biopsy.* Current treatment options in oncology, 2006. **7**(2): p. 141-151.

[4] Moncayo, V.M., et al. *Sentinel lymph node biopsy procedures*. in *Seminars in nuclear medicine*. 2017. Elsevier.

[5] Nagaraja, V., G.D. Eslick, and M.R. Cox, *Sentinel lymph node in oesophageal cancer—a systematic review and meta-analysis.* Journal of gastrointestinal oncology, 2014. **5**(2): p. 127.

[6] Wei, J. and Z. Bu, *Sentinel lymph node detection for gastric cancer: Promise or pitfall?* Surg Oncol, 2020. **33**: p. 1-6.

[7] Currie, A.C., *Intraoperative sentinel node mapping in the colon: potential and pitfalls.* European Surgical Research, 2019. **60**(1-2): p. 45-52.

[8] Narayanan, R. and T.G. Wilson, *Sentinel node evaluation in prostate cancer.* Clin Exp Metastasis, 2018. **35**(5-6): p. 471-485.

[9] Aljabery, F., et al., *Radio-guided sentinel lymph node detection and lymph node mapping in invasive urinary bladder cancer: a prospective clinical study.* BJU Int, 2017. **120**(3): p. 329-336.

[10] Accorsi, G.S., et al., *Sentinel Lymph Node Mapping vs Systematic Lymphadenectomy for Endometrial Cancer: Surgical Morbidity and Lymphatic Complications.* J Minim Invasive Gynecol, 2020. **27**(4): p. 938-945 e2.

[11] van de Loosdrecht, M.M., et al., *Laparoscopic Probe for Sentinel Lymph Node Harvesting using Magnetic Nanoparticles.* IEEE Transactions on Biomedical Engineering, 2021. **69**(1): p. 286-293.

[12] University_of_Twente, *Method and apparatus for detecting superparamagnetic material*. 2021: Patent pending.

[13] Waanders, S., et al., *Method and apparatus for measuring an amount of superparamagnetic material in an object*, in *Espacenet*. 2015: The Netherlands.

[14] van de Loosdrecht, M.M., et al., *Separation of excitation and detection coils for in vivo detection of superparamagnetic iron oxide nanoparticles.* Journal of magnetism and magnetic materials, 2019. **475**: p. 563-569.

[15] Pappalardo, F., et al., *In silico clinical trials: concepts and early adoptions.* Briefings in bioinformatics, 2019. **20**(5): p. 1699-1708.

[16] Hiruma, S., et al, *Eddy current analysis of litz wire using homogenization-based FEM in conjunction with integral equation.* IEEE Transactions on Magnetics, 2018. **54**(3): p. 1-4